

Investigations of structural, optical and electrical properties of Ca²⁺ doped CuCoO₂ nanosheets

Zijuan Du,^a Dehua Xiong,^{*,a} Jinchen Qian,^a Tianyang Zhang,^a Jilin Bai,^a De Fang^b and Hong Li^{*,a}

a. State Key Laboratory of Silicate Materials for Architectures, Wuhan University of Technology, Wuhan 430070, P. R. China

b. Center for Materials Research and Analysis, Wuhan University of Technology, Wuhan 430070, P. R. China

Email: xiongdehua2010@gmail.com (D. H. Xiong), lh_648@whut.edu.cn (H. Li).

Experimental details:**Preparation of delafossite oxide crystals of CCCaO nanosheets**

All chemicals in these experiments were purchased from Sinopharm Chemical Reagent Co.,Ltd and used without further purification. CuCoO_2 (CCO) nanocrystals and Ca doped CuCoO_2 (CCCaO) nanosheets were prepared according to our previous reports of hydrothermal procedure.^{1, 2} Generally, 20 mmol $\text{Cu}(\text{NO}_3)_2 \cdot 3\text{H}_2\text{O}$, $15x$ mmol $\text{Ca}(\text{NO}_3)_2 \cdot 4\text{H}_2\text{O}$ ($x = 0.03, 0.05, 0.10$), $15(1-x)$ mmol $\text{Co}(\text{NO}_3)_2 \cdot 6\text{H}_2\text{O}$ and 3.40 g NaOH were dissolved in 70 ml deionized water. Subsequently, the above solution was stirred at room temperature for a few hours. The precursor was then sealed in a 100 mL Teflon-lined autoclave to undergo a low-temperature (100 °C) hydrothermal reaction in a preheated oven. After the reaction kept for 24 h, the black-colored product was collected by centrifuging, and washed with aqueous ammonia solution, deionized water and ethanol in turn for several times. And then, the precipitates were stored in absolute ethanol for further characterizations.

Materials characterization

The crystal phase of samples was characterized by the powder x-ray diffraction (XRD, D8 Advance). The microstructure, morphology, and composition of as-synthesized CCO based samples were observed using the transmission electron microscopy (TEM, FEI Titan ChemiSTEM operating at 200 keV) coupled with energy-dispersive X-ray spectroscopy (EDX), and the field-emission scanning electron microscopy (FESEM, QUANTA FEG 450). These CCO based samples were deposited onto Cu grids coated with amorphous carbon for TEM examination, and the TEM characterizations were carried out using a Titan Themis TEM equipped with both probe and image Cs correctors and a Super-X EDS detector.^{3, 4} The mean particle size was detected by a laser granularity meter (Malvern M3600), operating with laser diffraction and previous ultrasonication of the synthesized CCCaO powders in deionized water. An atomic force microscopy (AFM) with DI Nanoscope IV controller (Veeco, USA)

was used to record the AFM height images of all these samples. The elements content of Cu, Co and Ca was quantified analysis by an inductively coupled plasma-optical emission spectrometry (ICP-OES, Prodigy 7). The X-ray photoelectron spectroscopy (XPS) data was collected by a physical electronics surface analysis equipment (ESCALAB250Xi), and the C (1s) line (at 284.80 eV) corresponding to the surface adventitious carbon (C–C line bond) has been used as the reference binding energy. The Brunauer-Emmett-Teller (BET) specific surface areas and porosity parameters of these CCO based samples were measured by N₂ adsorption desorption isothermometry (Micromeritics TriStar II 3020 3.02). The vibrational modes were recorded with a Raman spectroscope (LabRam HR Evolution) using a 532 nm excitation length at room temperature. The acquisition times ranged 10 s and the integral accumulations were 10 times. The optical absorption data of powder samples were monitored by Lambda 750 S (Perkin Elmer) at the spectral range 200-2500 nm, and BaSO₄ powder was used as the reflectance standard. Electrical conductivity was measured using the four-probe configuration (Tektronix 6517B), the dry powder of CCO based samples was pressed into a sheet with 0.8 cm diameter and 0.5 cm thickness using a tablet press machine (769YP-15A), and the temperature of the tableting samples was controlled by a temperature-controlled stage (Linkam HFS600E-PB2) from 0 to 300 °C with the heating rate of 2 °C min⁻¹.

Supplementary Tables:

Table S1. Average crystalline size measured by granulometric study and thicknesses of all CCO based samples measured by SEM and AFM.

Samples	Average crystalline size (nm)	Thickness of SEM measurement (nm)	Thickness of AFM measurement (nm)
CCO	540.0	85	45.8
CCCaO-1	507.6	55	20.3
CCCaO-2	498.8	20	17.4
CCCaO-3	488.4	15	13.7

Table S2. Chemical compositions of all CCO based samples deduced from ICP-OES measurements.

Samples	Co/Cu	Ca/Cu	Ca/(Cu+Ca)	Composition
CCO	1.136	0	0	$\text{CuCo}_{1.136}\text{O}_2$
CCCaO-1	0.961	0.010	0.010	$\text{Cu}_{0.990}\text{Ca}_{0.010}\text{Co}_{0.951}\text{O}_2$
CCCaO-2	0.938	0.018	0.018	$\text{Cu}_{0.982}\text{Ca}_{0.018}\text{Co}_{0.921}\text{O}_2$
CCCaO-3	1.147	0.034	0.033	$\text{Cu}_{0.967}\text{Ca}_{0.033}\text{Co}_{1.109}\text{O}_2$

Supplementary Figures:

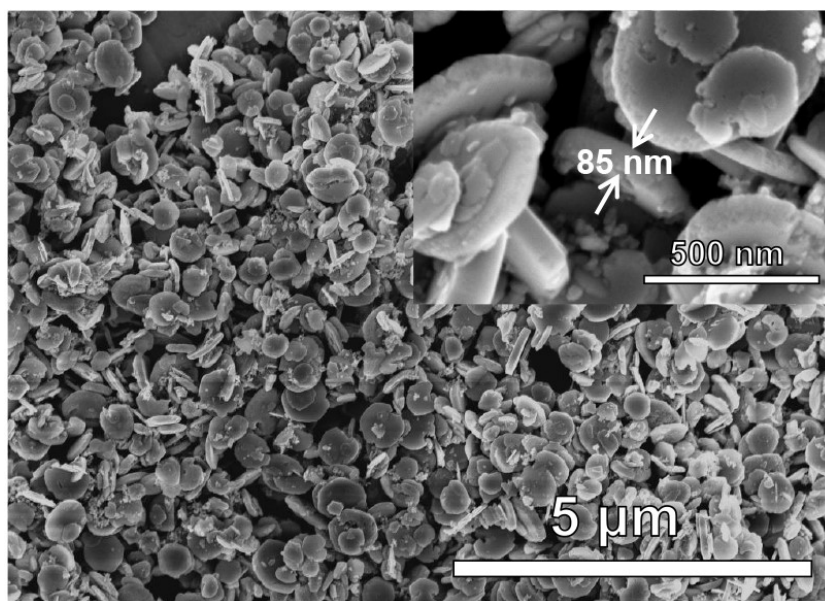


Fig. S1 SEM images of CCO nanocrystals.

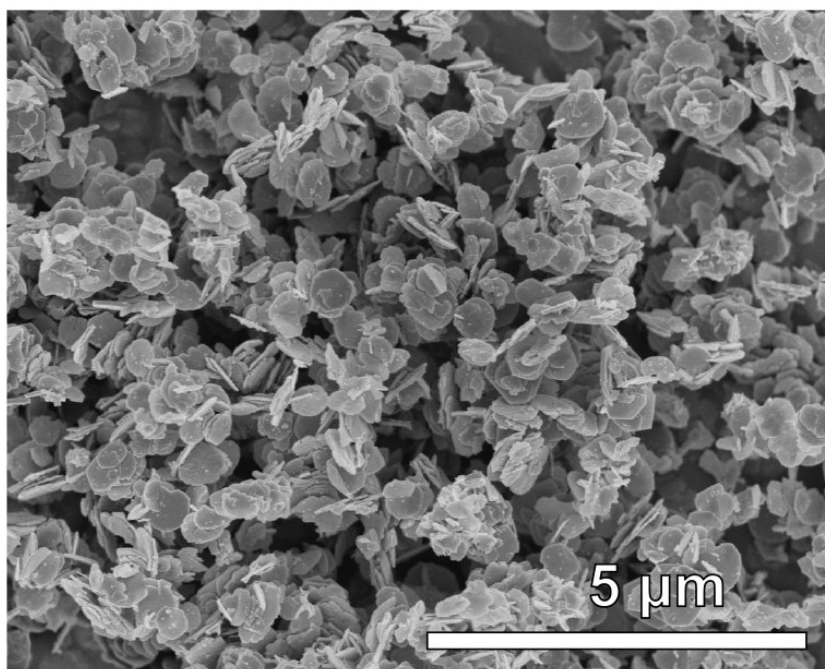


Fig. S2 SEM image of CCCaO-1 (3% - Ca doped) nanosheets.

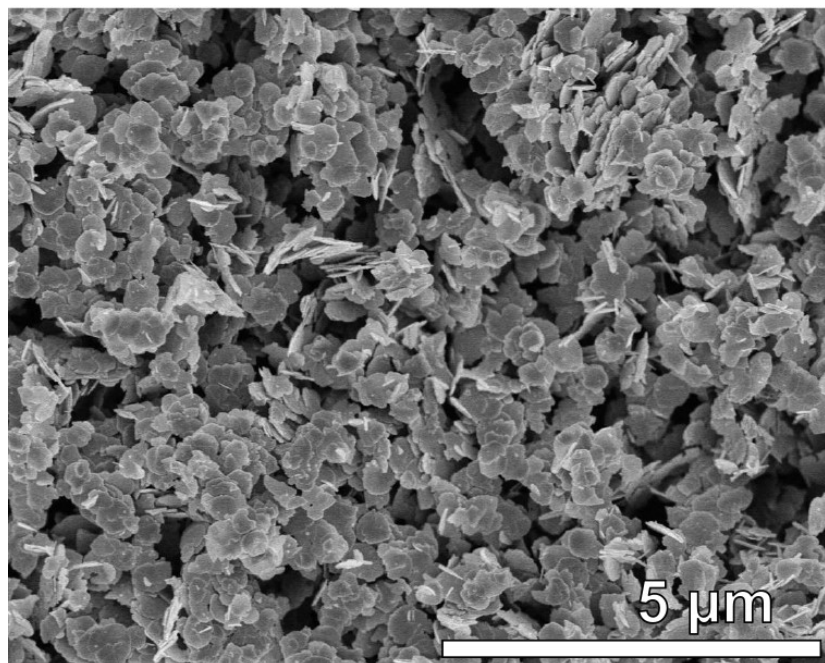


Fig. S3 SEM image of CCCaO-2 (5% - Ca doped) nanosheets.

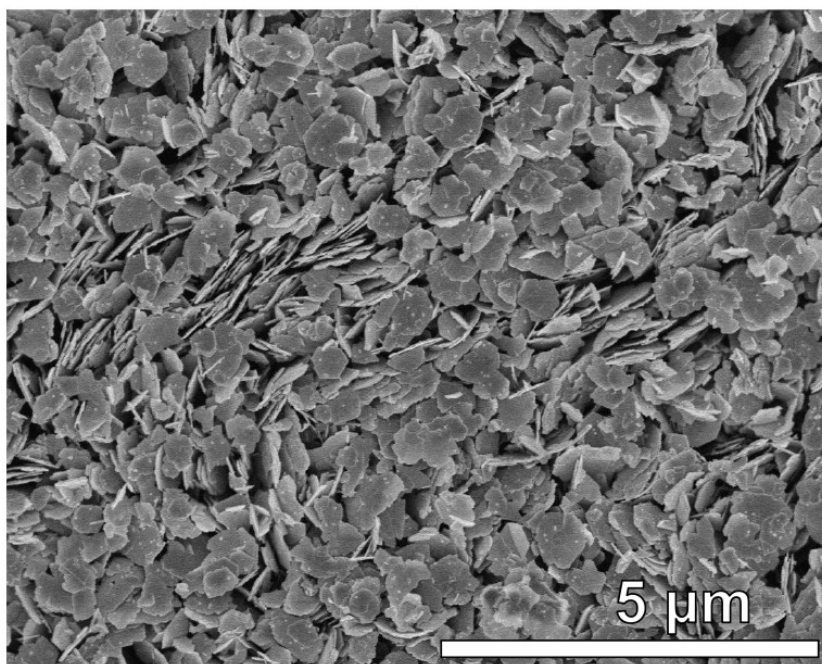


Fig. S4 SEM image of CCCaO-3 (10%- Ca doped) nanosheets.

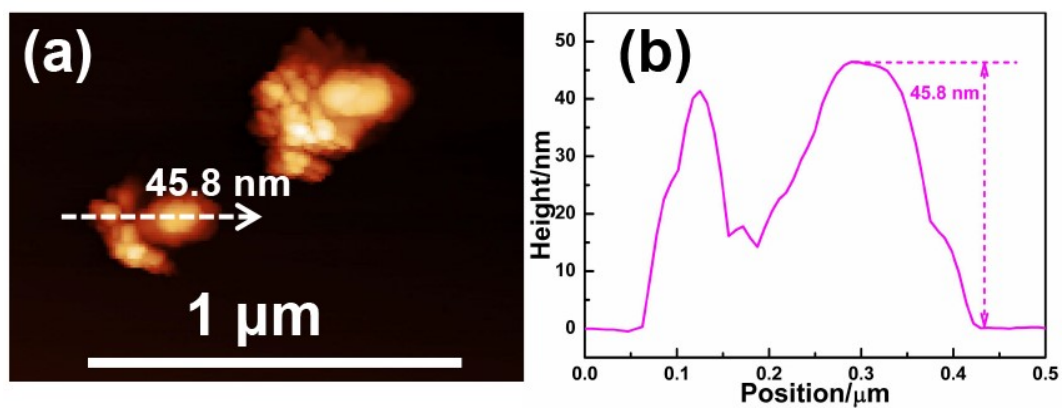


Fig. S5 AFM height image (a) and curve diagram (b) showing thickness distribution of CCO nanocrystals.

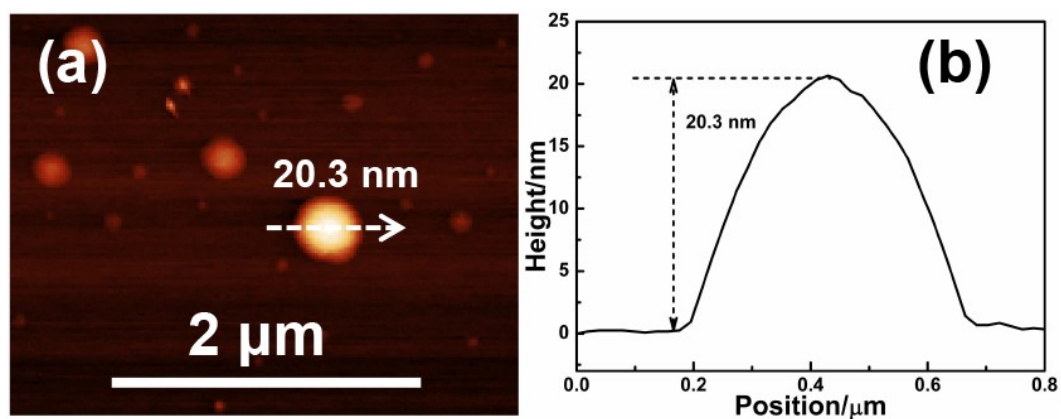


Fig. S6 AFM height image (a) and curve diagram (b) showing thickness distribution of CCCaO-1 nanosheets.

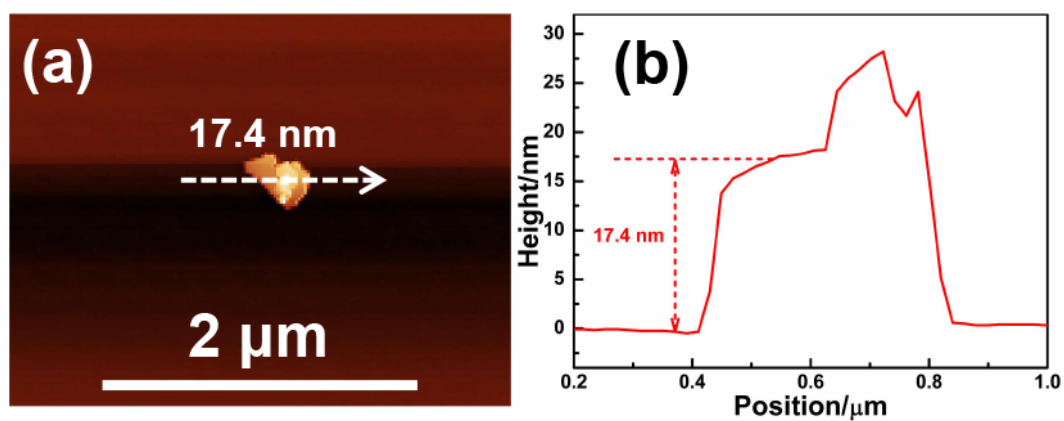


Fig. S7 AFM height image (a) and curve diagram (b) showing thickness distribution of CCCaO-2 nanosheets.

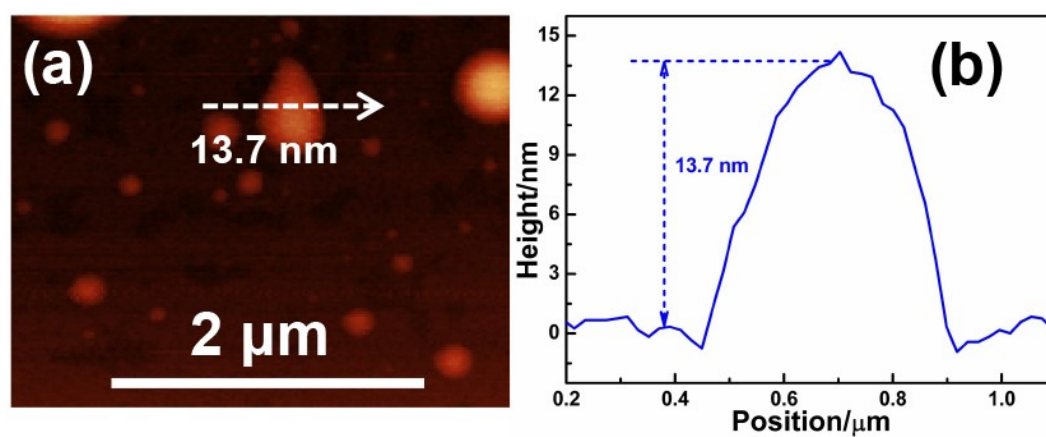


Fig. S8 AFM height image (a) and curve diagram (b) showing thickness distribution of CCCaO-3 nanosheets.

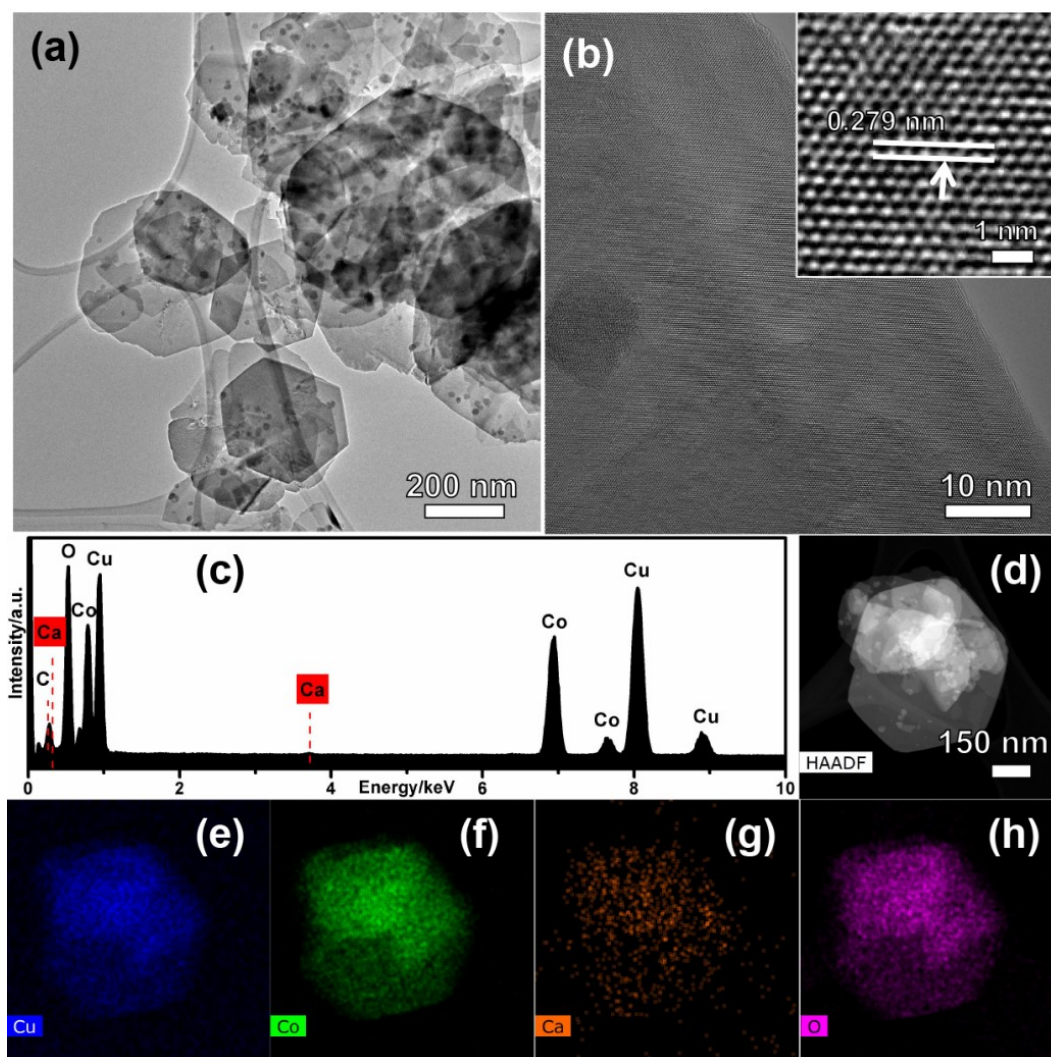


Fig. S9 TEM (a), HRTEM (b), EDX spectrum(c), HAADF-STEM (d), and elemental maps (e, Cu; f, Co; g, Ca; h, O) of CCCaO-1 nanosheets. The inset in (b) is zoomed view of lattice fringe.

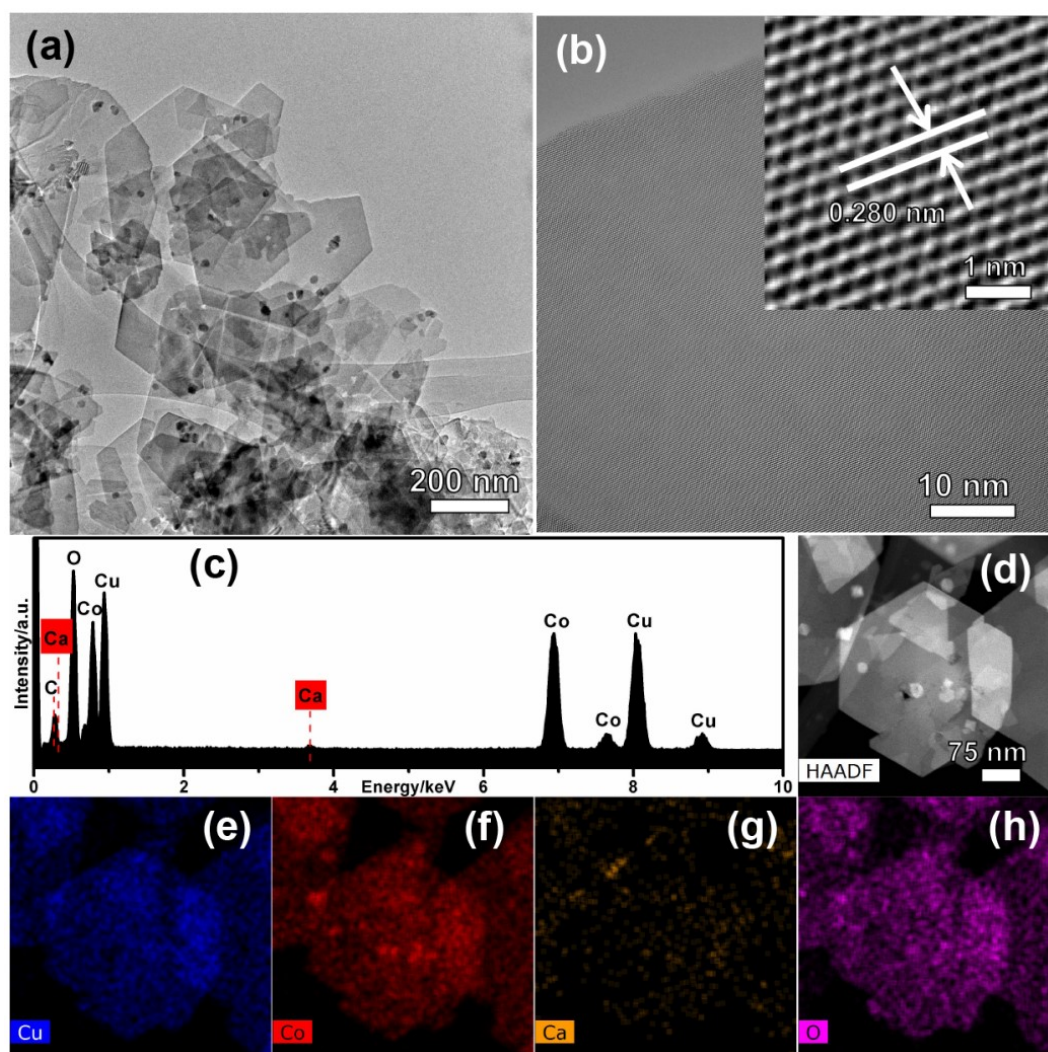


Fig. S10 TEM (a), HRTEM (b), EDX spectrum(c), HAADF-STEM (d), and elemental maps (e, Cu; f, Co; g, Ca; h, O) of CCCaO-3 nanosheets. The inset in (b) is zoomed view of lattice fringe.

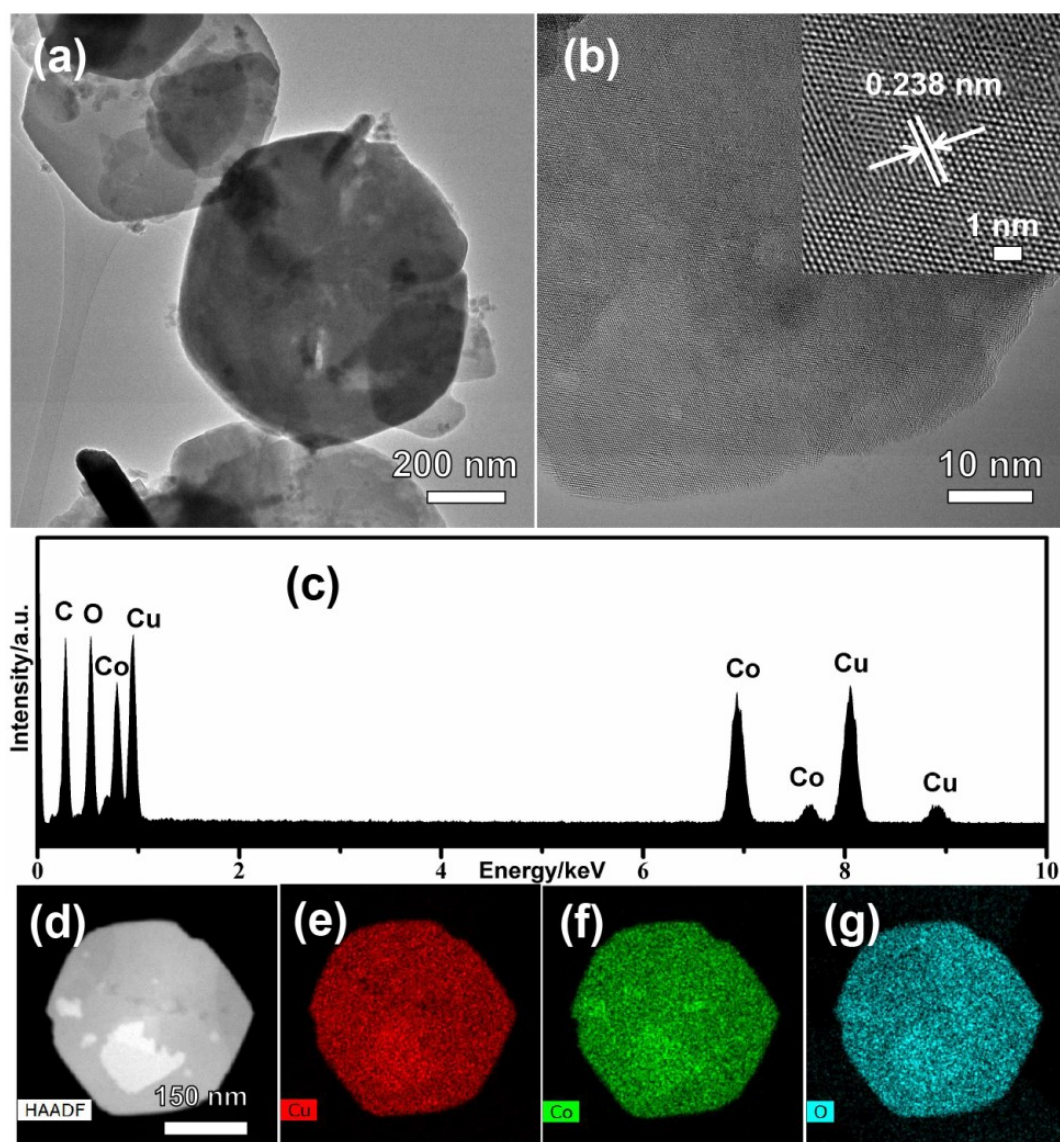


Fig. S11 TEM (a), HRTEM (b), EDX spectrum(c), HAADF-STEM (d), and elemental maps (e, Cu; f, Co; g, O) of optimized CCO nanocrystals. The inset in (b) is zoomed view of lattice fringe.

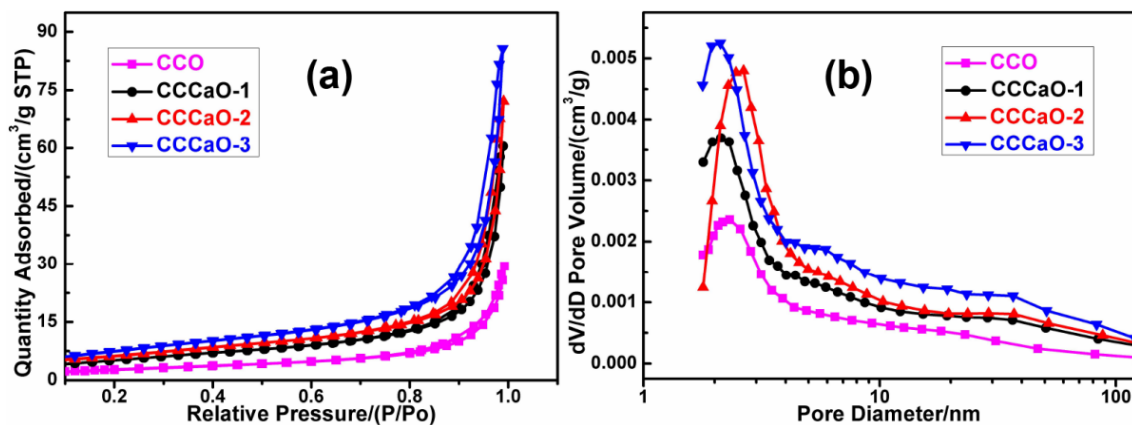


Fig. S12 Nitrogen adsorption/desorption isotherm plots (a) and BJH pore-size distribution curves (b) of CCO nanocrystals and CCCaO nanosheets.

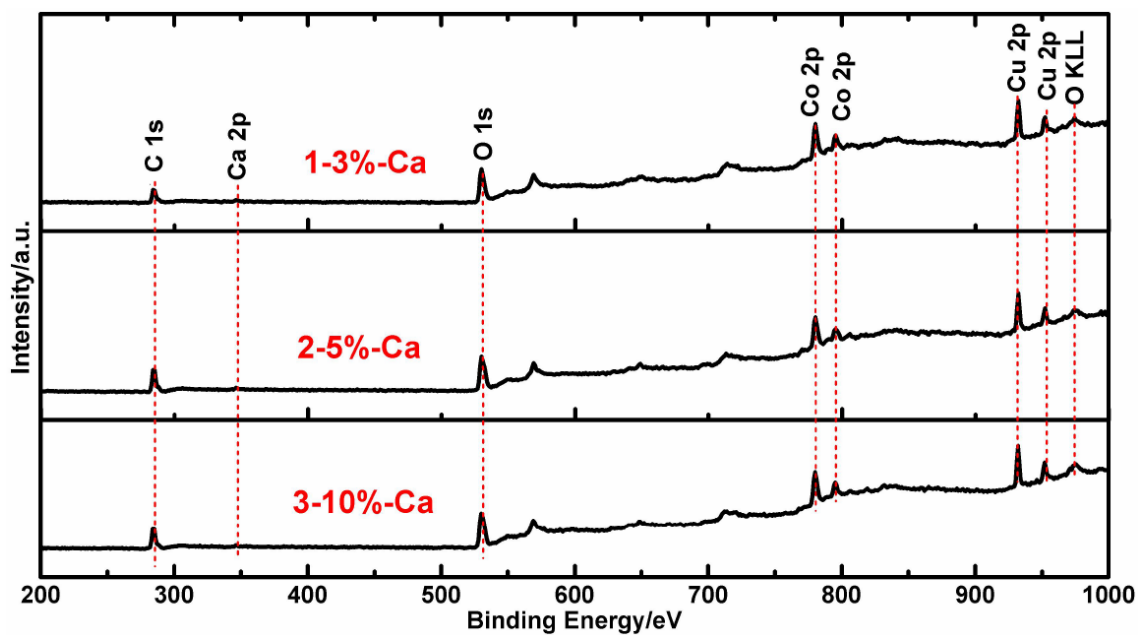


Fig. S13 XPS survey spectrum of CCCaO nanosheets.

References:

- [1]. D. Xiong, Z. Du, H. Li, J. Xu, J. Li, X. Zhao and L. Liu, *ACS Sustain. Chem. Eng.*, 2019, **7**, 1493-1501.
- [2]. D. Xiong, Q. Zhang, S. K. Verma, H. Li, W. Chen and X. Zhao, *J. Alloys Compd.*, 2016, **662**, 374-380.
- [3]. J. Li, J. Chen, H. Wang, N. Chen, Z. Wang, L. Guo and F. L. Deepak, *Adv. Sci.*, 2018, **5**, 1700992.
- [4]. J. Li, Z. Wang, Y. Li and F. L. Deepak, *Adv. Sci.*, 2019, **6**, 1802131.